Bulletin of the Seismological Society of America, Vol. 97, No. 6, pp. 1950–1959, December 2007, doi: 10.1785/0120060059

Stochastic Finite-Fault Modeling of Strong Ground Motions from the 26 December 2003 Bam, Iran, Earthquake

by Jafar Shoja-Taheri* and Hadi Ghofrani

Abstract On 26 December 2003, a destructive earthquake with an estimated M_w 6.5 occurred in southeastern Iran, causing extensive destruction in the city of Bam and its vicinity. The source of this shock was reported to have had a right-lateral strike-slip mechanism, and it initiated in a blind fault in the north–south direction. A regional network consisting of 23 strong motion stations (SSA-2 accelerographs) recorded the earthquake. The stations, located within 1–290 km of the epicenter, recorded peak ground accelerations between 0.01 and 0.99g. We employed the stochastic finite-fault method to simulate the recorded strong ground-motion data. The simulation is carried out using the Finite-Fault Simulation code (FINSIM) program (Beresnev and Atkinson, 1998a), which combines the stochastic ground-motion modeling technique with the kinematic model of rupture propagation. The fault is modeled as a rectangular plane with its area inferred from the distribution of the recorded aftershocks. The optimal size of the subfaults is selected as a function of the earthquake magnitude. Spectral analysis of the data indicates that the best match between the simulated and the observed spectra occurs for a radiation strength-factor of 1.6 and an average stress-parameter of 50 bars. The simulated peak amplitudes are in good agreement with the observed peaks. The observed and simulated spectra show a good agreement within the intermediate- and high-frequency ranges ($\geq$1 Hz) at all stations. However, at low frequencies, the recorded amplitude spectra are generally larger at most stations. This can be viewed as the limitation of the homogeneous half-space medium included in the simulation model to generate surface waves, which are generally observed on real accelerograms. Similar to the recorded data, the simulated records at the stations north of the source show larger peaks with shorter durations as compared with those south of the source. The simulation technique used in this study reproduces the effect of source directivity: a large and relatively long-period pulse arriving shortly after the onset of the *P*-wave at the Bam station.

Introduction

The Bam earthquake, one of the most destructive earthquakes in Iran's recorded history, occurred in the southeastern part of Iran at 01:56 UTC (05:26 local time) on 26 December 2003. The United States Geological Survey (USGS, http://earthquake.usgs.gov/) reported the epicenter at 29.004° N, 58.337° E, with a depth of 10 km and M_w 6.6. Using the recorded accelerograms (from the Building and Housing Research Center of Iran), the epicenter was located at 29.05° N, 58.37° E. According to several reports (e.g., Yamanaka, 2003; Yagi, 2003), the fault-plane solution of the mainshock and the spatial distribution of its aftershocks imply that this earthquake was produced by a right-lateral strike-slip fault with north–south strike and 88° dip to the west. This earthquake demolished more than 70% of the buildings in the city of Bam and its vicinity. It caused a death toll of more than 40,000 and injured about 30,000, as estimated by the local government (Statistics Center of Iran, 2004). The well-known historical citadel Arg-e-Bam, which is the biggest adobe structure in the world, was also severely damaged. An investigation of the recorded aftershocks (Nakamura *et al.*, 2004) showed that the hypocenters were distributed linearly over a 20 km long line, about 3.5 km west of the previously mapped Bam fault, extending from the south of Bam to the heavily damaged area in the eastern part of the city (see figure 1 of their article). The area of damage was relatively small for an earthquake of this size and was highly concentrated within the city of Bam and its vicinity.

*Present address: Building and Housing Research Center, Sheikh Fazlollah Expressway, P.O. Box 13145-1696, Tehran, Iran.

The most distinctive feature of the accelerograms recorded at the Bam site is the large and relatively long-period pulse recorded shortly after the *P*-wave arrival. This pulse of motion, which was the main cause of the extensive damage, represents the cumulative effect of nearly all of the seismic radiation energy from the fault rupture that nucleated at a point about 5 km south of the city and propagated northward (Shoja-Taheri *et al.*, 2005).

In the present study, we compute synthetic accelerograms for the Bam earthquake using the stochastic finite-fault technique. Our primary goal is to investigate the source parameters of this earthquake in some detail by matching the synthetic data with the general features of the recorded accelerograms. In addition, we want to see if this technique is also capable of reproducing the long-period pulse-shaped waveform recorded at the Bam station. Finally, we compare the synthetic peak ground accelerations (PGAs) with those predicted by the attenuation relation for the east-central region of Iran for M_w 6.5 (Shoja-Taheri *et al.*, 2005).

The simulation method used in this study is the stochastic finite-fault technique of Beresnev and Atkinson (1997, 1998a). In this method, the finite source is represented by a rectangular plane, subdivided into subfaults. Each subfault is treated as a point source and radiates an ω-squared spectrum. The ground motion at an observation point is obtained by summing the contributions of several subfaults. A simple kinematic model (Hartzell, 1978) is used to simulate the rupture propagation, which is assumed to start at the hypocenter and propagate out radially. Propagation effects are modeled by using the observed regional ground-motion amplitudes and durations as functions of distance.

Strong Motion Data

The data consist of 46 horizontal records obtained from a regional network of 23 three-component accelerograph stations (SSA-2) installed by the Iranian Strong Motion Network (ISMN) and maintained by the Building and Housing Research Center (BHRC; http://www.bhrc.gov.ir). The stations were located within 1–290 km of the epicenter. They recorded PGAs between 0.99 and 0.01g (see table 2 of Shoja-Taheri *et al.*, 2005). The recording stations, epicenter, and focal mechanism of the earthquake are shown in Figure 1.

The accelerograms were processed following the method used by Shoja-Taheri and Anderson (1988). The uncorrected data were originally digitized at the rate of 200 samples per second, but we processed the data at the

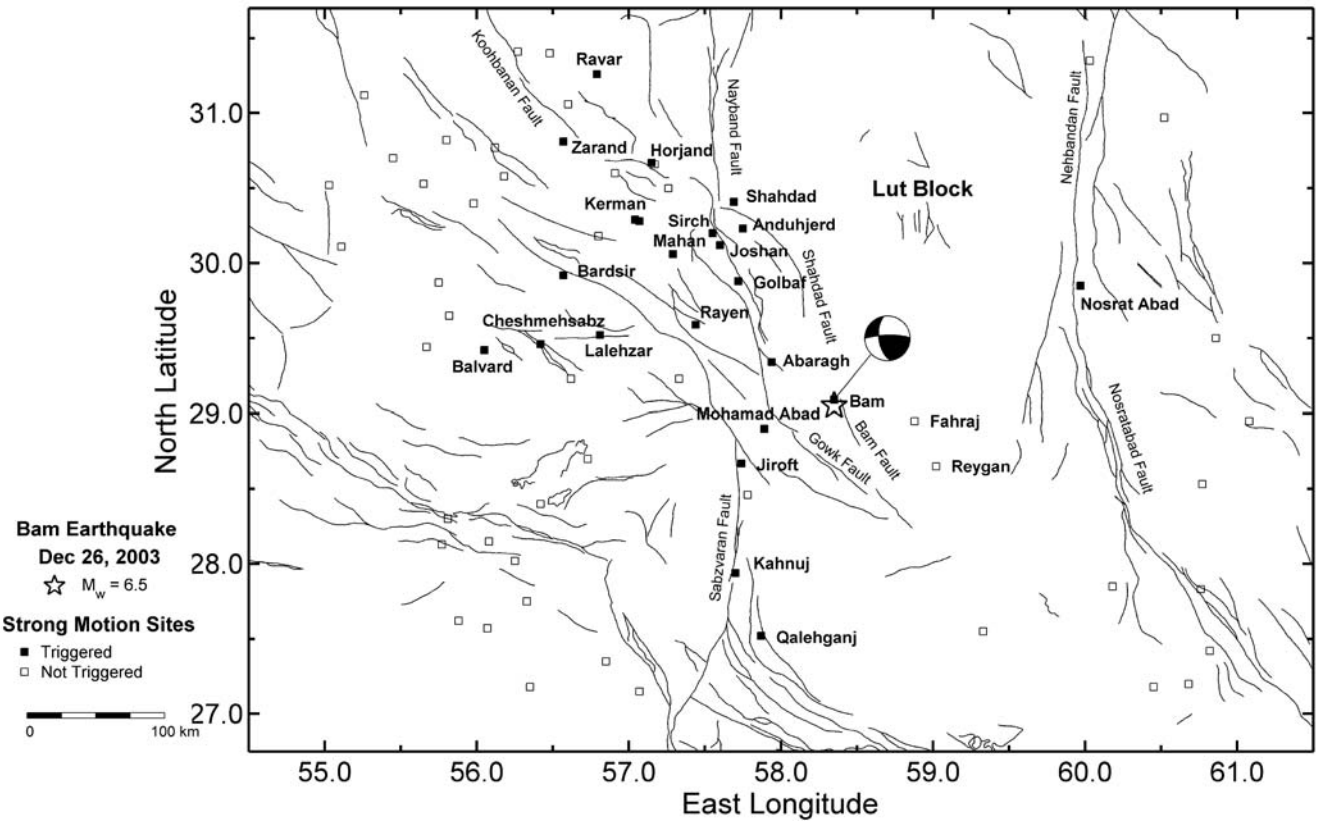

Figure 1. Regional map showing the epicenter (star) of the 2003 Bam earthquake and the recording stations (filled squares) used in this study. The focal mechanism of the mainshock is also shown.

rate of 100 samples per second. The accelerograms were passed through a four-pole high-pass zero-phase butterworth filter with corner frequency of 0.125 Hz.

Modeling Parameters

In the method of Beresnev and Atkinson (1997, 1998a), modeling of the finite source requires the orientation and dimensions of the fault plane, the dimensions of subfaults, and the location of the hypocenter. The parameters used in this study are listed in Table 1. Orientation of the fault model is derived from the focal mechanism of the 2003 Bam mainshock, reported by Yamanaka (2003). Dimensions of the fault were chosen based on the spatial distribution of the aftershocks, recorded during the first two days after the earthquake (IIEES, 2003). The subfault size is one of the most crucial parameters used in almost all simulation techniques. It is shown to increase linearly with moment magnitude **M** (Beresnev and Atkinson, 1999):

$$\mathrm{Log}\Delta l = -2.08 + 0.416\mathbf{M} \qquad (4 \le \mathbf{M} \le 8), \qquad (1)$$

where Δl is the subfault size in kilometers. As indicated by Beresnev and Atkinson (2002), this relationship reduces the epistemic uncertainty by empirically constraining the subevent size, leaving only aleatory uncertainty due to the event-to-event scatter about the mean. We set the subfault size to the precise size of 5 km in order to make the simulation reasonably independent of the subfault size (Beresnev and Atkinson, 1998a). The corner frequency of the radiated ω-square spectrum (f_c) and the corresponding subfault moment (m_0) are derived from the subfault size:

$$f_c = \frac{(yz/\pi)\beta}{\Delta l}, \qquad (2)$$

$$m_0 = \Delta\sigma\Delta l^3, \qquad (3)$$

where β is the shear-wave velocity, y is the ratio of rupture velocity to β, normally set to a value of 0.8, and z is the product of strength factor (sfact) and 1.68, a value that holds for a standard rupture. The parameter sfact controls the amplitudes of the radiation at frequencies larger than the corner frequency of the subfaults and has been linked to the maximum velocity of slip on the fault (Beresnev and Atkinson, 1998a). A value of sfact equal to 1.0 corresponds to a slip with moderate rupture velocity. We tested different values of sfact in the range 0.4–2.0 and found that the best match between simulated and observed spectra was obtained for sfact = 1.6. In equation (3), $\Delta\sigma$ is a stress parameter, or a coefficient relating subfault moment to its size. This parameter controls each subfault moment and also the total moment summed over all subsources. As recommended by Beresnev and Atkinson (1997) to avoid an inadequate number of active subsources, the stress parameter is set to a value of 50 bars, the average static stress drop as introduced by Kanamori and Anderson (1975).

In the simulation, the effects of the propagation path are modeled using geometrical spreading, anelastic, and near-surface attenuations. For geometrical attenuation we assumed the spreading factor of R^{-1} for distances up to 100 km, to account for the expected amplitude decrease of body waves, and $R^{-0.5}$ for distances larger than 100 km, to account for surface waves (Herrmann and Kijko, 1983).

Attenuation of pseudoacceleration response spectra of horizontal records is estimated at particular frequencies in the band 0.25–8.0 Hz. This allows for finding the spectral amplitude decay associated with the assumed bilinear form of geometrical spreading. Following Atkinson and Mereu (1992), we tested all possible combinations of the attenuation parameters, by generating random numbers bounded by the physical ranges for each of them, and then searched for the combination that minimizes the average residual errors (see Shoja-Taheri *et al.*, 2007). The frequency-dependent anelastic coefficient, k, is related to the quality factor, Q, by

$$Q = \frac{[\log(e)\pi f]}{k(f)\beta}.$$

Based on the estimated values of k, the mean frequency-dependent quality factor of $Q(f) = 352.73 \pm 0.87 f^{1.052\pm0.028}$ is obtained (Fig. 2). In this figure, the regional mean Q^{-1}-values determined in this study are shown as open squares, and the best-fit curve to these values is shown as a dotted line.

Table 1
Modeling Parameters

Parameter	Parameter Value
Fault orientation	strike 178°; dip 85°
Fault dimensions along strike and dip	20 by 15 km
Fault depth range	0–15 km
Mainshock moment	6.3096E+25 dyne cm
Subfault dimensions	5 by 5 km
Stress parameter	50 bars
Radiation strength factor	1.6
Subfault moment	9.3750E+24 dyne cm
Number of subfaults	12
Subsources summed	$6.7303 \approx 7$
Subfault rise time	0.9470 sec
Subfault corner frequency	0.3953 Hz
Duration (T_d)	$T_0 + 0.05R$
$Q(f)$	$352.73f^{1.052}$
Geometrical spreading	$(1/R)$, $R \le 100$ km $(100R)^{-1/2}$, $R > 100$ km
Windowing function	Saragoni-Hart
High-cut filter	κ values per second
Crustal shear-wave velocity	3.3 km/ sec
Rupture velocity	0.8 × (shear-wave velocity)
Crustal density	2.7 g/cm^3

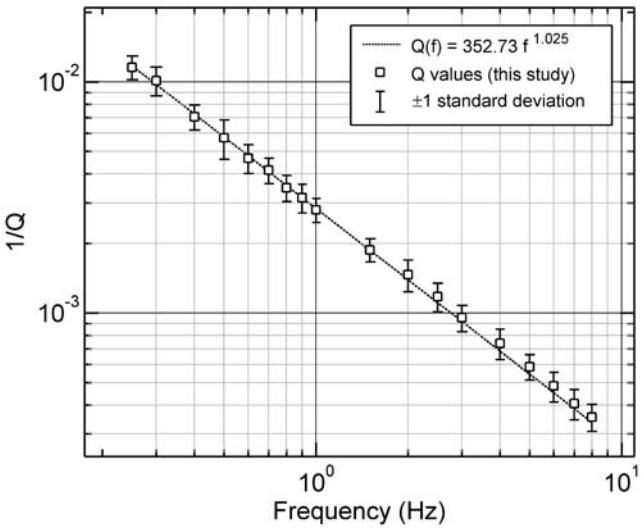

Figure 2. Regional mean Q^{-1}-values (squares) determined in this study from analyzing pseudoacceleration response spectra. Bars are indicating ± 1 standard deviations of the mean values at each frequency. The best-fit curve determined in the present work has been shown as a dotted line.

High-frequency amplitudes are reduced by near-surface attenuation through the κ operator (Anderson and Hough, 1984). The spectrum is multiplied by the factor $\exp(-\pi\kappa f)$, where κ is the near-surface spectral decay parameter. We used the κ values evaluated by Shoja-Taheri *et al.* (2005) from the spectra of the horizontal accelerograms recorded during the Bam earthquake. As depicted in Figure 13 of their article, κ values generally increase with distance R as $\kappa = 0.00023R + 0.035$.

The duration model has the following form:

$$T = T_0 + bR, \tag{4}$$

where T_0 is the source duration ($f_0 = 1/T_0$ is the corner frequency of the Brune [1970] model) and R is the hypocentral distance. For the distance-dependent term, we used $b = 0.05$ (Herrmann, 1985).

Reliable simulations of ground-motion amplitudes require that the site response at each recording station be taken into account. To estimate the site amplification at each station, we used both the standard spectral ratio (SSR) (Borcherdt, 1970) and the horizontal-to-vertical ratio (H/V) techniques (Nakamura, 1989). Following Jarpe *et al.* (1988), the relative site response, corrected for the different attenuation and geometric spreading for sites 1 and 2, is given by

$$\frac{S_1}{S_2} = \frac{g_1}{g_2}\frac{G(r_1)}{G(r_2)}e^{\pi(r_1-r_2)f/\beta Q}. \tag{5}$$

In this equation, S_1/S_2 is the "true" site response or the ratio between the horizontal amplitude spectrum at a soil site (S_1) and that of the corresponding spectrum at the rock site (S_2), g_i is the smoothed average horizontal spectrum of the ground motion, $G(r_i)$ is the geometrical spreading factor, r_i is the hypocentral distance, f is the frequency, Q is the quality factor, and β is the shear-wave velocity. For the computation of SSR, the bilinear model for geometric spreading was included.

Among all the stations that recorded the Bam earthquake, Rayen is the only station located on rock (see figure 1 and table 2 of Shoja-Taheri *et al.* [2005]). Therefore, site amplifications at all other stations were estimated by comparing their recorded spectra with the spectra recorded at the Rayen site. Figure 3 shows the results of both the SSR and H/V techniques. Previous results (e.g., Bard, 1998; Castro *et al.*, 2001) have shown that the H/V technique usually underestimates site amplifications. For this reason, we consider the results given by SSR to be more reliable.

Results

Results of finite-fault simulations are validated against the recorded horizontal accelerations and their corresponding Fourier amplitude spectra. Figure 4 shows the horizontal components of the recorded accelerograms and their corresponding simulated time series. The simulated time series at each station is a single random horizontal component. PGAs are generally well reproduced. Figure 4 also shows the Fourier spectra of the simulated records (dark solid lines) together with the observed average spectra (dotted lines). We have limited our analysis to the frequency band of 0.25–8.0 Hz to avoid signal-to-noise ratios greater than three. The observed and simulated spectra show a good agreement within the intermediate- and high-frequency ranges (≥ 1 Hz) at all stations. At low frequencies, the recorded amplitude spectra are generally larger at most stations. This can be explained by the fact that the homogeneous half-space medium included in the simulation model could not generate surface waves, which are generally observed on real accelerograms.

The distinctive feature of the time histories recorded at the Bam site is the relatively long-period pulse-shape waveform, which was recorded shortly after the onset of *P* wave (Figs. 4 and 5). Propagation of a rupture toward a site at a velocity that is almost as large as the shear velocity causes most of the seismic energy from the rupture to arrive in a single large pulse of motion that occurs at the beginning of the record (Somerville *et al.*, 1997). The energy in this pulse of ground acceleration accounts for almost all of the seismic energy generated on the entire fault. In addition, the radiation pattern of shear dislocation on the fault causes this large pulse of motion to be oriented in the direction perpendicular to the fault (Aki and Richards, 1980). Forward rupture directivity effects occur when two conditions are met: the rupture front propagates toward the site, and the direction of slip on the fault is aligned with the site. In the case of strike-slip faulting, the conditions for generating forward rupture directivity are met where the fault slip direction is oriented horizontally along strike, either unilaterally or bilaterally (Somerville and Grave, 1993; Somerville *et al.*, 1997).

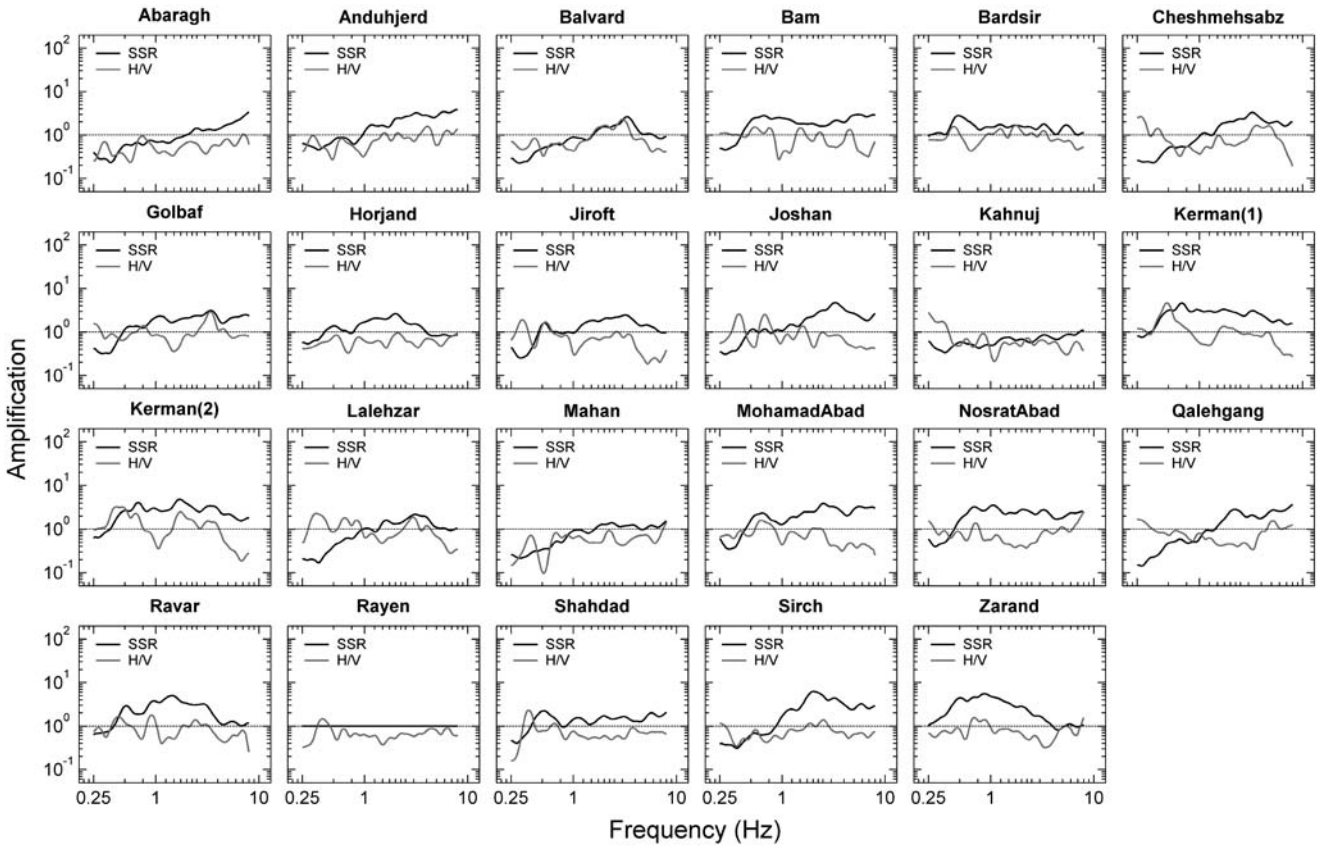

Figure 3. Comparison between site amplification factors at the 23 stations that recorded the Bam earthquake, estimated by H/V (gray lines) and SSR (dark lines) techniques.

In the case of the Bam earthquake, it is believed (Shoja-Taheri *et al.*, 2005) that the rupture was nucleated in the blind fault about 5 km south of the city of Bam and propagated northward, passing the Bam site where it was recorded as a long-period pulse at this station. As shown in Figure 5, the waveform synthesized by the simulation for this site resembles the effect of observed directivity in both amplitude and period.

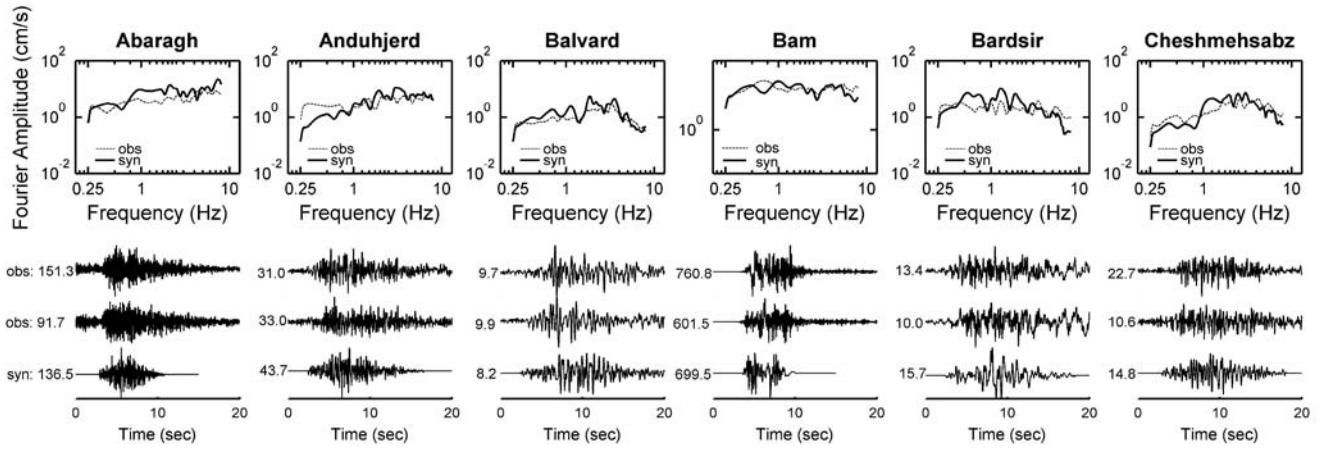

Figure 4. Recorded and simulated accelerograms with their corresponding peak values (cm/ sec^2). The dotted line is the average Fourier amplitude spectrum of the observed horizontal components, and the dark solid line is the acceleration spectra calculated from the simulated time histories. The two upper traces are the observed horizontal accelerations, longitudinal and transversal components, respectively.
(*Continued*)

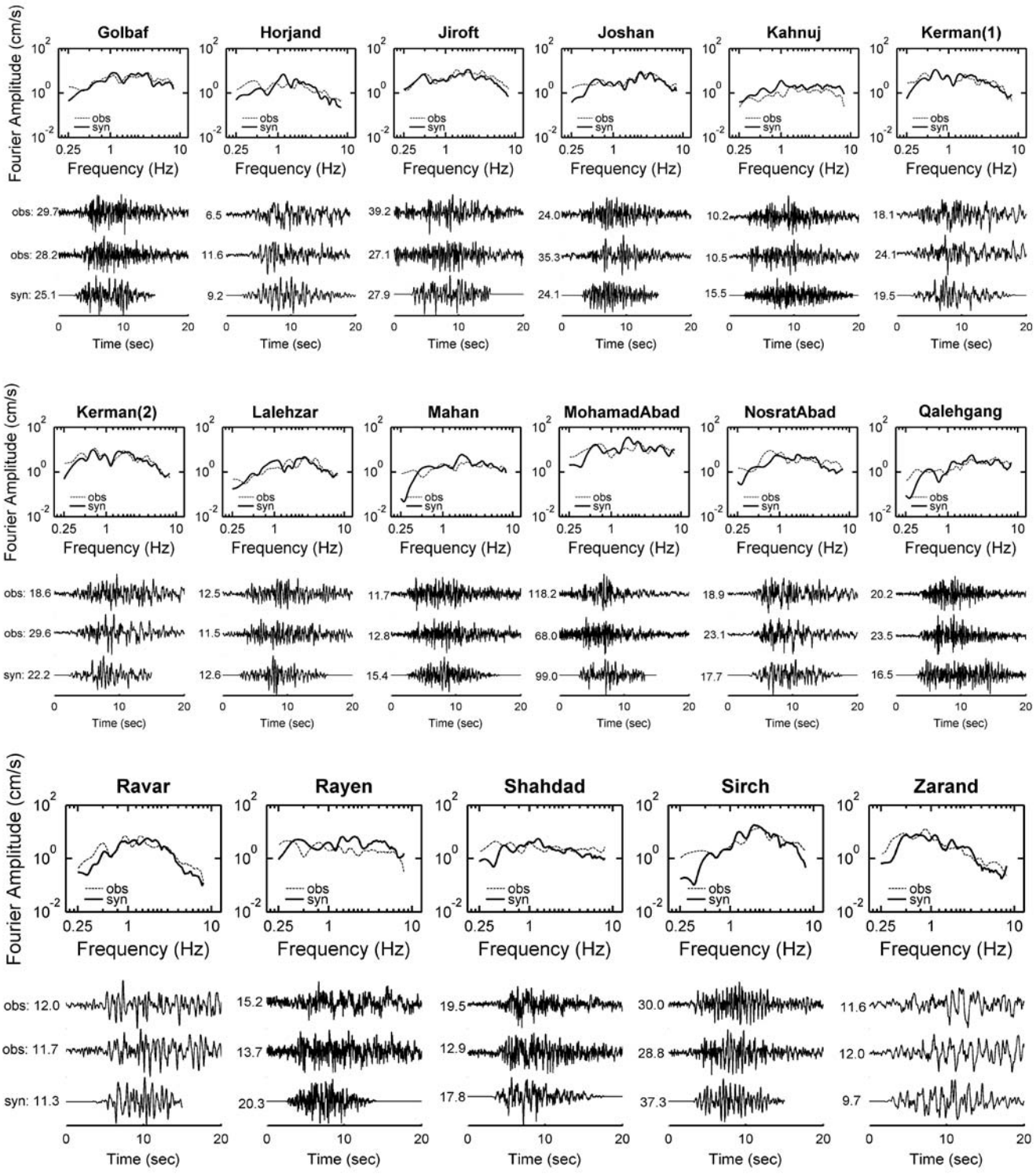

Figure 4. Continued.

The model bias is commonly defined as the mean of the ratio between the simulated and the observed Fourier spectra, taken over all stations (Abrahamson *et al.*, 1990; Schneider *et al.*, 1993; Atkinson and Boore, 1998). The mean, the 95% confidence limit, and the standard deviation estimated for different spectra are shown in Figure 6. The standard deviation provides a measure of the prediction uncertainty for individual stations, while the confidence limit

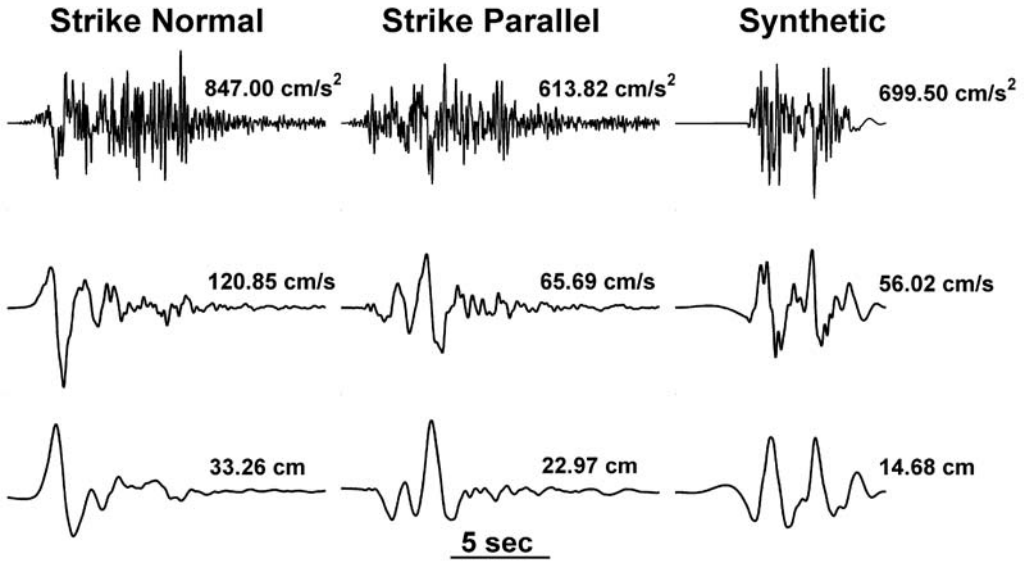

Figure 5. Observed (strike normal and strike parallel) and synthetic time series at the Bam site. As shown, the relatively long-period pulse shape of about 2 sec is visible on the simulated record. The peak values are also shown for comparison between the synthetic and recorded records. Velocity and displacement records are obtained by integrating the acceleration time series.

gives an estimate of prediction uncertainty bias of the model (Beresnev and Atkinson, 1998b). It is observed that the mean ratio of the simulated to the observed spectra is not significantly different from unity at frequencies larger than 1 Hz.

Figure 7 shows ratios of the synthetic PGA and the observed geometric mean of the horizontal components versus epicentral distances for all stations. Figure 8 depicts the corresponding ratios of peak spectral acceleration values for the periods of 0.125 and 2.0 sec. The close agreements between the observed and synthetic ground motions indicate that the attenuation model and the mean amplification factors employed in the simulation have been well estimated. Uncertainties in predictions at individual sites are shown in Figure 9.

Attenuation Relations of the Synthetic Ground Motion

Relations describing peak ground motions and response spectral amplitudes as functions of earthquake magnitudes and distances are essential in the assessment of earthquake hazard analyses. For large magnitudes there are not many motion data near the source. The recorded motion at the Bam site could provide a significant contribution to modifing attenuation relations at near source distances. The large peaks at the Bam site lead to significant differences between the attenuation curves developed by adding the Bam earthquake data (Shoja-Taheri *et al.*, 2005) and those previously developed for the east-central region of Iran for M_w 6.5 (Shoja-Taheri, 2002). However, it should be noted that the comparison between the relations will be justified only when the effect of source directivity at the Bam site is removed from the recorded motions.

To compare the attenuation of the synthetic ground motions with the attenuation relation for the region (Shoja-Taheri *et al.*, 2005), we simulated accelerograms for nearly 5000 nodes in a mesh covering the area shaken by this earthquake. We assumed that all the stations in the area are located on rock. We fitted the simulated PGAs using

$$\log(Y) = C_1 + C_2 \log(R) + C_3 R \pm \sigma,$$
$$R = (x^2 + h^2)^{1/2}. \quad (6)$$

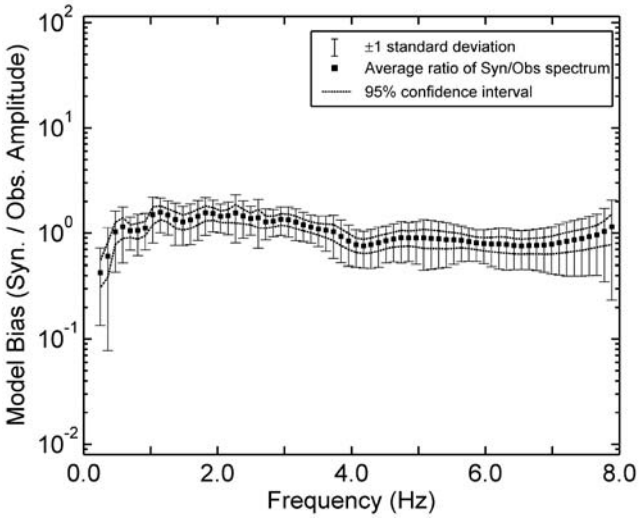

Figure 6. Model bias showing the ratio of the simulated to the observed spectra averaged over all stations (filled squares in Fig. 1). The observed spectrum at each site is calculated as the geometric average of spectra of two horizontal components. Bars show ±1 standard deviations

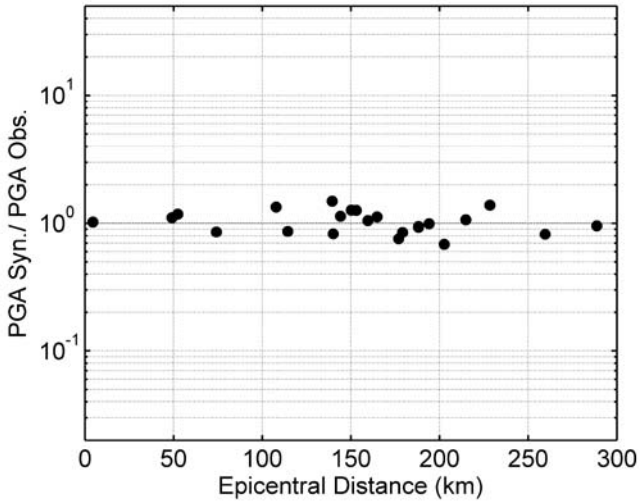

Figure 7. Ratio of simulated to observed (average of two horizontal components) PGA as a function of epicentral distance.

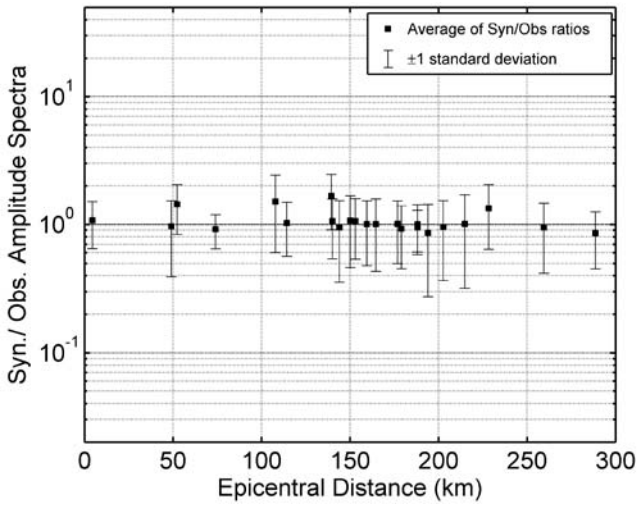

Figure 9. Uncertainties in predictions at individual sites. The filled symbols are mean values for the frequency range of 0.25–8.0 Hz, and the bars are ±1 standard deviation of averaged ratios of observed to synthetic spectral amplitude versus epicentral distance at the 23 examined stations.

Here Y is the peak value of ground motion, x is the nearest distance to the fault surface, $h = 5.0$ km is a fictitious depth that was selected for the Bam data to be consistent with the shallow depth of about 5 km inferred (Shoja-Taheri *et al.*, 2005), σ is the standard error of regression, and C_1, C_2, and C_3 are the coefficients to be determined by the regression. The estimated coefficients are listed in Table 2. The standard deviation, σ, is estimated to be 0.10. In Figure 10, the synthetic peaks for distances between 1 and 60 km from the epicenter are plotted. The peaks are compared with the 50% PGA prediction curve by Shoja-Taheri *et al.* (2005) for M_w 6.5 (dotted line). The prediction curve derived from synthetic data is shown with a solid line. Despite the simplicity of the model, there is consistency between the synthetic and the observed ground-motion relations (Table 2). At the near source distances, the synthetic peaks at the nodes north of the epicenter are noticeably larger than those at the southern nodes. These differences decrease gradually with the increasing epicentral distances. We interpret this observation as the effect of the northward rupture propagation during the earthquake.

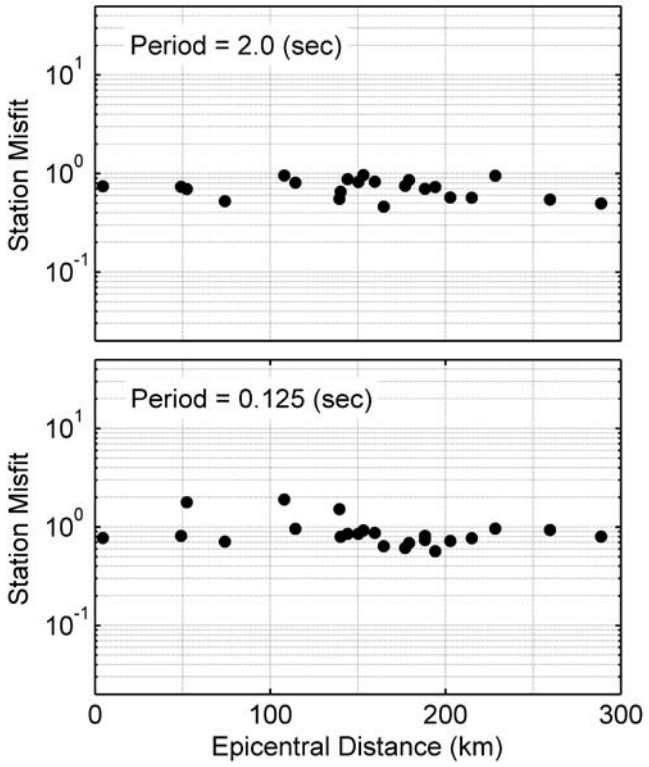

Figure 8. Station misfit (ratio of simulated to observed spectrum) as a function of epicentral distance. Misfits are shown at representative periods of 2.0 and 0.125 sec.

Conclusions

Horizontal ground-motion accelerograms of the M_w 6.5 2003 Bam, Iran, earthquake were simulated using the stochastic finite-fault modeling technique (Beresnev and Atkinson, 1997, 1998a). The results show the good agreement between the simulated and the observed peak amplitudes (Fig. 7). Also, the ratio of the simulated to the observed spectrum in the used frequency range, averaged over all recording sites, is not significantly different from the unity within the 95% confidence interval (Fig. 6). However, the homogeneous half-space medium assumed in the simulation model limits the generation of surface waves that are generally observed on the real accelerograms. This causes the recorded amplitude spectra at low frequencies to generally be larger than those spectra produced by the

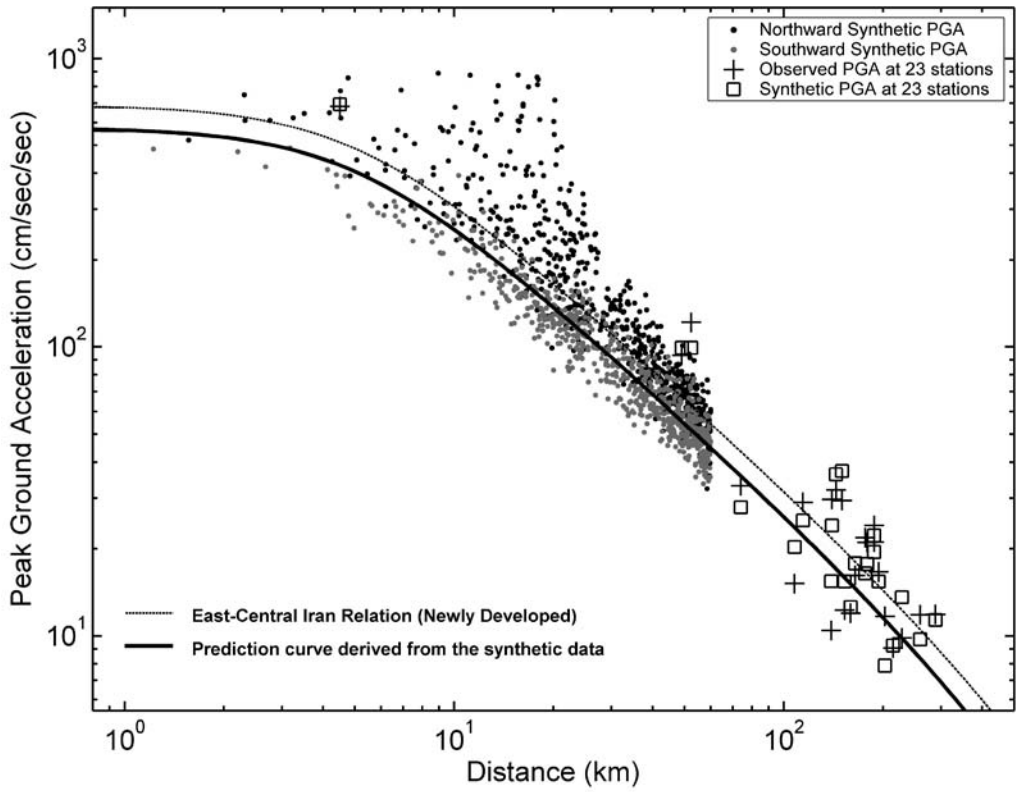

Figure 10. Comparison between the 50% PGA prediction curve derived by Shoja-Taheri *et al.* (2005) for the east-central region of Iran for M_w 6.5 (dotted line) and the attenuation curve derived from the synthetic data (solid line). The square and plus symbols are the synthetic and the observed peaks, respectively, at the 23 recording sites. The small circles show only those synthetic data within the distances close to the epicenter. It is noteworthy that at the near source distances the synthetic peaks at northern points of the epicenter are noticeably larger than those at the southern points.

simulation at most stations. Because of the existence of small-scale heterogeneities in the earthquake source process and crustal properties, the effects of source radiation and wave propagation become increasingly incoherent at short periods. Therefore, it is difficult to determine the effects of small-scale heterogeneities of the path and the source when the simulation technique is used in the range of high frequency. The model was tested with different slip distributions that are reported from teleseismic observations and also with the random generation of moment distributions with varying nucleation points. The best match between the simulated and observed spectra is obtained when the hypocenter is set at the middle of the main fault with random distribution of slip. The adopted model was able to reproduce the effect of near-field directivity, which is observed as a long-period pulse of ground motion at the Bam site (Fig. 5). This effect is also noticeable when the comparison is made between the synthetic peaks at the points near and on the opposite sides of the epicenter. The simulated acceleration spectra at the individual stations show large errors. These errors result from the uncertainties in the estimation of mean transfer functions and other factors such as surface topography or complexity of the source. The attenuation curve of the synthetic peaks at dummy stations shows good agreement with the empirical curves (Fig. 10).

Table 2

Comparison between Synthetic and Observed Ground-Motion Relations

Parameter	C_1	C_2	C_3
Observed PGA	3.539	−1	−0.00040
Synthetic PGA	3.460	−1	−0.00048
	±0.004	(Fixed)	±2.25E − 005

Acknowledgments

We thank Gail M. Atkinson and Igor Beresnev for allowing us to use their simulation code (FINSIM). We are also grateful to Dariush Motazedian and Rasool Anooshehpoor for their helpful comments on this article. An anonymous reviewer and the associate editor Francisco J. Chávez-García are also acknowledged for their constructive comments and suggestions. This work was partially supported by the Building and Housing Research Center of the Ministry of Housing and Urban Development of Iran. The strong motion data used in this project were provided by the National Strong Motion Network of Iran.

References

Abrahamson, N. A., P. G. Somerville, and C. A. Cornell (1990). Uncertainty in numerical strong motion predictions, in *Proceedings of the 4th U.S. National Conference on Earthquake Engineering*, Palm Springs, California, Vol. 1, 407–416.

Aki, K., and P. G. Richards (1980). *Quantitative Seismology: Theory and Methods*, W. H. Freeman, New York.

Anderson, J. G., and S. E. Hough (1984). A model for the shape of the Fourier amplitude spectrum of acceleration at high frequencies, *Bull. Seismol. Soc. Am.* **74,** 1969–1993.

Atkinson, G. M., and D. M. Boore (1998). Evaluation of models for earthquake source spectra in eastern North America, *Bull. Seismol. Soc. Am.* **88,** 917–934.

Atkinson, G. M., and R. F. Mereu (1992). The shape of ground motion attenuation curves in southeastern Canada, *Bull. Seismol. Soc. Am.* **82,** 2014–2031.

Bard, P. Y. (1998). Microtremor measurements: a tool for site effect estimation?, in *Proceedings of the 2nd International Symposium on Effects of Surface Geology on Seismic Motion*, Yokohama, Japan, 1–3 December 1998, Vol. 3, 1251–1282.

Beresnev, I. A., and G. M. Atkinson (1997). Modeling finite-fault radiation from the ω^n spectrum, *Bull. Seismol. Soc. Am.* **87,** 67–84.

Beresnev, I. A., and G. M. Atkinson (1998a). FINSIM-a FORTRAN program for simulating stochastic acceleration time histories from finite faults, *Seism. Res. Lett.* **69,** 27–32.

Beresnev, I. A., and G. M. Atkinson (1998b). Stochastic finite-fault modeling of ground motions from the 1994 Northridge, California, earthquake. I. validation on rock sites, *Bull. Seismol. Soc. Am.* **88,** 1392–1401.

Beresnev, I. A., and G. M. Atkinson (1999). Generic finite-fault model for ground-motion prediction in eastern North America, *Bull. Seismol. Soc. Am.* **89,** 608–625.

Beresnev, I. A., and G. M. Atkinson (2002). Source parameters of earthquakes in eastern and western North America based on finite-fault modeling, *Bull. Seismol. Soc. Am.* **92,** 695–710.

Borcherdt, R. D. (1970). Effects of local geology on ground motion near San Francisco Bay, *Bull. Seismol. Soc. Am.* **60,** 29–61.

Brune, J. N. (1970). Tectonic stress and the spectra of seismic shear waves, *J. Geophys. Res.* **75,** 4997–5009.

Castro, R. R., A. Rovelli, M. Cocco, M. Di Bona, and F. Pacor (2001). Stochastic simulation of strong-motion records from the 26 September 1997 (M_w 6), Umbria-Marche (Central Italy) earthquake, *Bull. Seismol. Soc. Am.* **91,** 27–39.

Hartzell, S. H. (1978). Earthquake aftershocks as Green's functions, *Geophys. Res. Lett.* **5,** 1–4.

Herrmann, R. B. (1985). An extension of random vibration theory estimates of strong ground motion to large distances, *Bull. Seismol. Soc. Am.* **75,** 1447–1453.

Herrmann, R. B., and A. Kijko (1983). Modeling some empirical vertical component *Lg* relations, *Bull. Seismol. Soc. Am.* **73,** 157–171.

International Institute of Earthquake Engineering and Seismology (IIEES) (2004). Preliminary Report of Bam Earthquake, www.iiees.ac.ir/English/bank/Bam/Bam_report_english.html (last accessed October 2006).

Jarpe, S. P., C. H. Cramer, B. E. Tucker, and A. F. Shakal (1988). A comparison of observations of ground response to weak and strong ground motion at Coalinga, California, *Bull. Seismol. Soc. Am.* **78,** 421–435.

Kanamori, H., and D. L. Anderson (1975). Theoretical basis of some empirical relations in seismology, *Bull. Seismol. Soc. Am.* **65,** 1073–1095.

Nakamura, Y. (1989). A method for dynamic characteristics estimation of subsurface using microtremor on the ground surface, *Q. Rep. Railw. Tech. Res. Inst.* **30,** 25–33.

Nakamura, T., S. Suzuki, T. Matsushima, Y. Ito, S. Keivan Hosseini, A. J. Gandomi, H. Sadeghi, M. Maleki, and S. M. Fatemi Aghda (2004). Source fault structure of the 2003 Bam earthquake, southeastern Iran, inferred from the aftershock distribution and its relation to the heavily damaged area: existance of the Arg-e-Bam fault proposed, 2004, *Geophys. Res. Lett.* **32,** no. 9, L09308.

Schneider, J. F., W. J. Silva, and C. Stark (1993). Ground motion model for the 1989 *M* 6.9 Loma Prieta earthquake including effects of source, path, and site, *Earthquake Spectra* **9,** 251–287.

Shoja-Taheri, J. (2002). Attenuation relations for peak and response spectra of horizontal acceleration from strong-motion records for the main seismic zones of the Iranian Plateau (Abstract), *Seism. Res. Lett.* **73** (SSA Meet. Suppl.), 242.

Shoja-Taheri, J., and J. G. Anderson (1988). The 1978 Tabas, Iran, earthquake: an interpretation of the strong motion records, *Bull. Seismol. Soc. Am.* **78,** 142–171.

Shoja-Taheri, J., S. Nasserrieh, and A. H. Ghafoorian-nasab (2005). The 2003 Bam, Iran, earthquake: an Interpretation of the strong motion records, *Earthquake Spectra* **21,** S181–S206.

Shoja-Taheri, J., S. Nasserrieh, and H. Ghofrani (2007). M_L and M_W scales in the Iranian Plateau based on the strong-motion records, *Bull. Seismol. Soc. Am.* **97,** 661–669.

Somerville, P. G., and R. W. Grave (1993). Conditions that give rise to unusually large long period ground motion, *Struct. Des. Tall Build.* **2,** 211–232.

Somerville, P. G., N. F. Smith, R. W. Grave, and N. A. Abrahamson (1997). Modification of empirical strong ground motion attenuation relations to include the amplitude and duration effects of rupture directivity, *Seism. Res. Lett.* **68,** 199–222.

Statistics Center of Iran (2004). Number of fatalities, casualties, and missing people as a result of the Bam earthquake, 2004, available at http://amar.sci.org.ir/Detail.aspx?Ln=F\&no=201638 (in Persian) (last accessed March 2005).

Yagi, Y. (2003). Preliminary results of rupture process for 2003 December 26 southeastern Iran, earthquake, source process of recent large earthquakes, International Institute of Seismology and Earthquake Engineering, http://iisee.kenken.go.jp/staff/yagi/eq/Iran20031226/IRAN20031226.htm (last accessed October 2005).

Yamanaka, Y. (2003). Seismological Note: No. 145, Earthquake Information Center, Earthquake Research Institute, University of Tokyo, http://www.eri.u-tokyo.ac.jp/sanchu/Seismo_Note/EIC_News/031226w.jpg (last accessed October 2005).

Earthquake Research Center (EQRC)
Ferdowsi University
P.O. Box 9177948974
Mashad, Iran
j-shoja@seismo.um.ac.ir
ghofrani@seismo.um.ac.ir

Manuscript received 18 March 2006